Influences of nanoparticles and chain length on thermodynamic and electrical behavior of fluorine liquid crystals

Ines Ben Amor1, Lotfi Saadaoui1,†, Abdulaziz N. Alharbi2, Talal M. Althagafi2, and Taoufik Soltani1

Citation: Chin. Phys. B, 2022, 31 (**10**): 104202. DOI: 10.1088/1674-1056/ac7293
Journal homepage: http://cpb.iphy.ac.cn; http://iopscience.iop.org/cpb

What follows is a list of articles you may be interested in

Compact 2×2 parabolic multimode interference thermo-optic switches based on fluorinated photopolymer

Ji-Hou Wang(王继厚), Chang-Ming Chen(陈长鸣), Ke-Wei Hu(胡珂玮), Ru Cheng(程儒), Chun-Xue Wang(王春雪), Yun-Ji Yi(衣云骥), Xiao-Qiang Sun(孙小强), Fei Wang(王菲), Zhi-Yong Li(李智勇), Da-Ming Zhang(张大明)
Chin. Phys. B, 2019, 28 (**4**): 044207. DOI: 10.1088/1674-1056/28/4/044207

Improved dielectric and electro-optical parameters of nematic liquid crystal doped with magnetic nanoparticles

Geeta Yadav, Govind Pathak, Kaushlendra Agrahari, Mahendra Kumar, Mohd Sajid Khan, V S Chandel, Rajiv Manohar
Chin. Phys. B, 2019, 28 (**3**): 034209. DOI: 10.1088/1674-1056/28/3/034209

Structural, vibrational, optical, photoluminescence, thermal, dielectric, and mechanical studies on zinc (tris) thiourea sulfate single crystal: A noticeable effect of organic dye

Mohd Shkir, V Ganesh, S AlFaify, I S Yahia, Mohd Anis
Chin. Phys. B, 2018, 27 (**5**): 054216. DOI: 10.1088/1674-1056/27/5/054216

Enhanced thermal stability of VCSEL array by thermoelectric analysis-based optimization of mesas distribution

Chu-Yu Zhong(钟础宇), Xing Zhang(张星), Di Liu(刘迪), Yong-Qiang Ning(宁永强), Li-Jun Wang(王立军)
Chin. Phys. B, 2017, 26 (**6**): 064204. DOI: 10.1088/1674-1056/26/6/064204

Influences of nanoparticles and chain length on thermodynamic and electrical behavior of fluorine liquid crystals

Ines Ben Amor[1], Lotfi Saadaoui[1,†], Abdulaziz N. Alharbi[2], Talal M. Althagafi[2], and Taoufik Soltani[1]

[1] *Université Tunis El Manar, Laboratoire de Physique de la Matière Molle et de la Modélisation Electromagnétique, 2092 Tunis*
[2] *Physics Department, College of Science, Taif University, P. O. Box 11099, Taif 21944, Saudi Arabia*

(Received 13 March 2022; revised manuscript received 28 April 2022; accepted manuscript online 24 May 2022)

Hydrogen-bonded polar nematic liquid crystal series with the general formula *n*OBAF ($n = 7$–12) is studied. The mesomorphic characterization is demonstrated through differential scanning calorimetry (DSC) and polarized optical microscopy (POM). The complexes with short alkyl chains ($n = 7$, 8) present a wide nematic range and monotropic smectic F mesophase, whereas the longer alkyl chain ($n = 10$–12) analogues show high melting and low clearing mesomorphic liquid crystals. The thermal range of the mesophase and the birefringence increase with chain length decreasing. Furthermore, the effect of the nanoparticles ($LiNbO_3$) on the thermal and the electrical behavior of 8OBAF are investigated. The presence of $LiNbO_3$ nanoparticles increases the conductivity and reduces the resistivity of the complex.

Keywords: fluorine liquid crystal, polar nematic, ferroelectric nanoparticles, thermal stability, dielectric behavior

PACS: 42.70.Df, 61.30.Eb, 61.30.–v **DOI:** 10.1088/1674-1056/ac7293

1. Introduction

The originality of liquid crystals lies in the fact that it is very easy to act on their structure by external physical agents. Liquid crystals were present more than a century ago out of purely academic interest, owing to long efforts, new effects of considerable technological importance have been observed. The study of these materials has experienced rapid development since the 1970s. In the majority of thermotropic liquid crystals generally made up of organic compounds, the cohesion is ensured by Van der Waals, dipolar or hydrophilic/hydrophobic interactions. Relatively lower in energy, these interactions have little or no specificity, no stoichiometry, and no directivity, in contrast to quantum forces, a large part of energy exists in covalent bonds.

With an intermediate value of energy and a specific and reversible character, other intermolecular interactions such as hydrogen bonds allow self-assembly of complementary molecules, and thus leading the supramolecular liquid crystal to be obtained.[1–12] Aromatic carboxylic acids were often utilized in the preparation of hydrogen bonding liquid crystals (HBLC's). Nowadays, H-bonded liquid crystal is being widely explored especially for their easy synthetic process and wide potential applications. Indeed, it can be used in various optical and electro-optical devices such as liquid crystal capacitors, optical storage of data, optical filters in the visible and infra-red region.[13] Most of HBLC mesogens are made from symmetric and non-symmetric dimers of molecules showing nematic and smectic phases.[14–20] Several complexes have been obtained through intermolecular hydrogen bonding including systems consisting of derivatives of benzoic acid as hydrogen bond donors and pyridine moieties as hydrogen bond acceptors.[21–23] In addition, hydrogen-bonded LC polymers with interesting behaviors have also been obtained.[24–27] Several reports have discussed the influence of the structure on the thermal stability and mesomorphic phase sequence of the material of this type. It has been found that lateral substituent with different sizes and polarities widely improves many properties of liquid crystalline materials.[14] Another element that can affect the mesophase range of the liquid crystals is the chain of the compounds. Hagar *et al.*[28] have demonstrated that the isotropic–nematic phase transition temperature and the entropy ΔS_{IN} increase with chain length increasing. Another way to create nanomaterials with desired behaviors is to prepare the nanocomposite based on liquid crystal matrix doped with numerous types of nanoparticles including semiconductor,[29–31] ferromagnetic,[32,33] and ferroelectric.[34–36] By doping antiferroelectric liquid crystal with $BaTiO_3$ nanoparticles, Lalik *et al.* have obtained ions capturing, low viscosity, a drop in threshold voltage and spontaneous polarization, due to faster molecular switching.[36] Ayeb *et al.* have also used semiconductor nanoparticles to modify liquid crystal properties and have shown that after doping with 5CB with Cu–TiO_2 nanoparticles, the isotropic–nematic phase transition temperature increases by almost 2 °C, and the optical and dielectric anisotropy is also observed.[31]

Our efforts devote to the understanding of the relationship between the chemical structure and physical properties of the fluorinated liquid crystalline materials.[17,37] This work represents the continuation of the studies of HBLCs with alkyloxy benzoic group, with an aim to obtain the cybotactic nematic phase that can be applied to electro-optical devices and photonics. Synthesis of compounds under the study has been

†Corresponding author. E-mail:lotfi.saadaoui@fst.utm.tn

presented earlier.[37] The objective of the present work is to study the effect of the chain length on mesomorphic, dielectric, and structural properties. In addition, we present the influence of $LiNbO_3$ nanoparticles with diameter about 150 nm on the physical properties of the 8OBAF ($n = 8$) liquid crystalline matrix.

2. Materials and methods

The liquid crystal materials used in the present study were 4-(n alkyloxy)-3-fluoro benzoic acid (nOBAF) with $n = 7$–12 (as shown in Fig. 1).

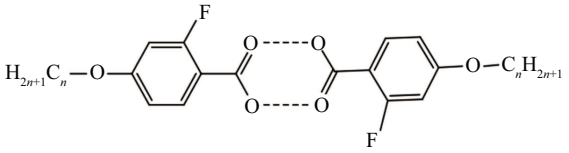

Fig. 1. General chemical formula of the compounds under study ($n = 7$–12).

The general phase sequences of 8OBAF, 10OBAF, and 12OBAF were described in Refs. [17,37]. The complexes were characterized by differential scanning calorimetry (DSC) and POM. The measured DSC thermograms were obtained in heating and cooling cycle with a scan rate of 5 °C/min. The mesophases were identified by the POM. The compounds were loaded into ITO electro-optical cells with 8 μm in thickness by capillary action at the isotropic temperature of the LC. The filled cell was cooled slowly and the alignment of the sample was checked under crossed polarizes. Optical textural observations were made with a polarizing optical microscope (POM) (Olympus BX51) equipped with a digital charge coupled device (CCD) camera (Sony). The temperature was controlled within ±1 °C/min. The LC textures were processed, analyzed and stored with aid of imaging software (Archimed). General chemical formula of the compounds under study is shown in Fig. 1.

The ferroelectric nanoparticles $LiNbO_3$, which purchased from Merck were used in this study as dopant. The $LiNbO_3$ has a spherical shape and average size about 150 nm. The mixture of 8OBAF and the NPs with 1 wt% was prepared.

3. Results and discussion

3.1. Host liquid crystalline material

3.1.1. Thermal stability

The thermal behaviors and the phase transition temperatures are investigated by using the DSC thermograms as shown in Fig. 2. The hydrogen-bonded complex DSC thermograms are obtained during heating and cooling cycles with the same scan rate 10 °C/min. For 7OBAF and 8OBAF, the cooling scan of the DSC thermogram reveals four transitions: isotropic (I)–nematic (N), nematic (N)–smectic C (Sm C), smectic C (Sm C)–smectic F (Sm F), and Smectic F (Sm F)–crystal (Cr), with transition temperatures at 118 °C, 93 °C, 53 °C, and 45 °C for 7OBAF and 115.8 °C, 96.5 °C, 75.3 °C, and 56 °C for 8OBAF, respectively. Besides, the heating cycle shows for 7OBAF three distinct transitions from Cr → SmC→ N→ I at 86 °C, 101.6 °C, 121.8 °C, and two transitions for 8OBAF from Cr → N→ I at 92 °C, respectively. These transition temperatures are in consistence with the POM observations. Figures 3(a)–3(c) show the textures of the nematic phase, the SmC phase, and the SmF phase, respectively. It should be mentioned that the SmF phase is observed only on the cooling scan which is a monotropic mesophase.

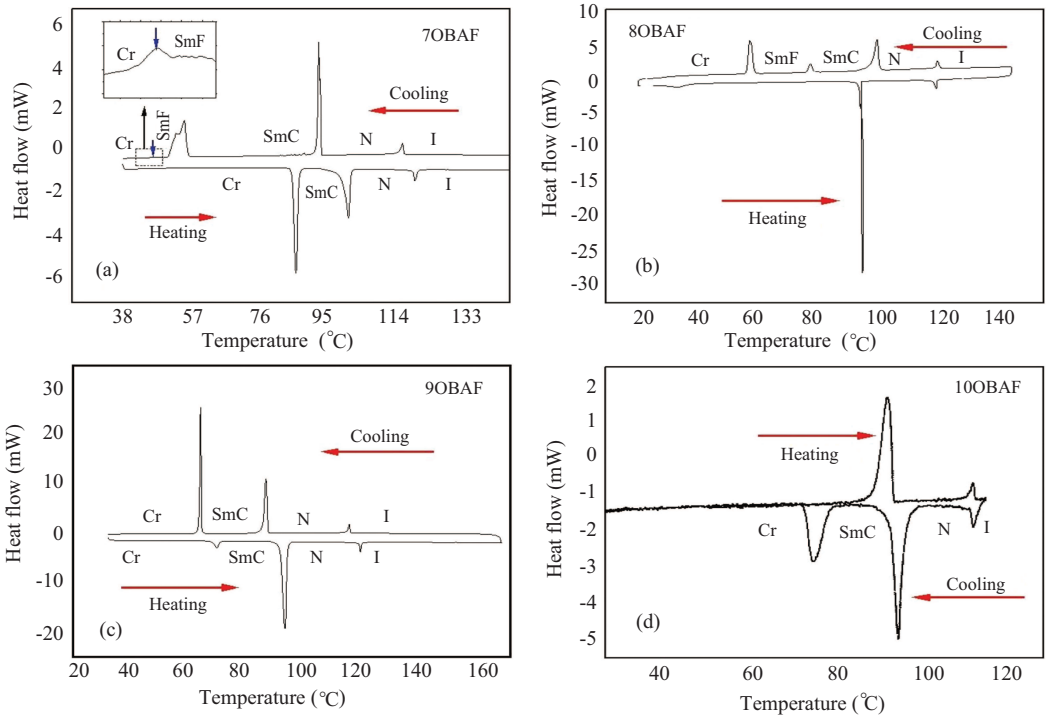

Fig. 2. DSC curves during heating and cooling scan for nOBAF.

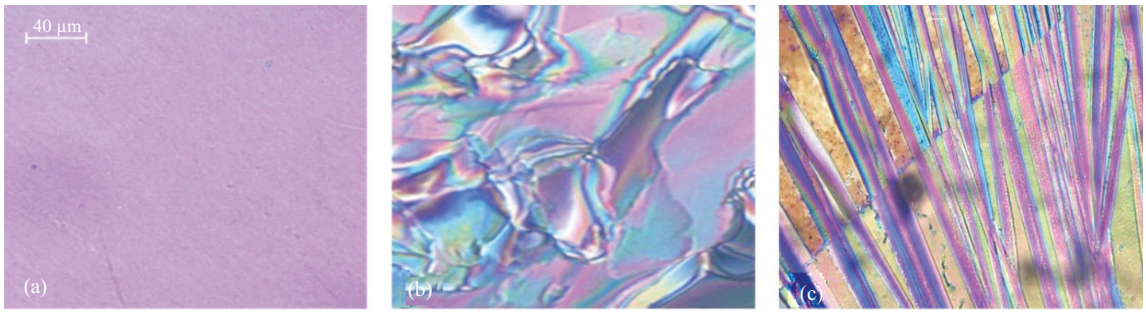

Fig. 3. Polarized optical microscopy textures of the phases obtained in complexes: (a) nematic phase, (b) SmC phase, and (c) SmF phase.

The other complexes *n*OBAF ($n = 9$, 10, 11, and 12) reveal only the nematic and the SmC phases during the heating and the cooling scan.

Figure 4 shows the phase transition temperatures with respect to chain length. The highest clearing temperature (119.5 °C) is obtained for 7OBAF. Moreover, 12OBAF possesses the highest melting temperature at 87 °C and the lowest clearing point temperature of 109 °C, respectively. Such characteristics show that a shorter carbon chain length gives appealing mesomorphic quality through a lower melting point temperature and, in particular, a wide temperature range of the nematic phase. Remarkably, the melting point temperature does not decrease as the carbon chain length increases. As is common with all compounds, SmC phase is observed. The number of carbon atoms has no discernible effect on the inhibition of SmC. However, the compounds $n = 7$ and $n = 8$ are most favorable to have the SmF mesophase. Increasing the length of the carbon chain reduces the clearing temperature substantially. As a result, the length of the flexible alkyl chain plays a role in suppressing the SmF phase and lowering the clearing point.

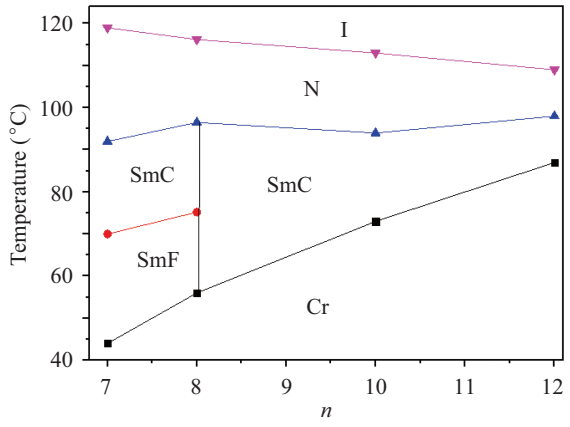

Fig. 4. Plot of transition temperatures against alkyl chain lengths (n).

Obviously, the primary consequence in these series is a significant push towards a less ordered system as the length grows. Thus, as n steadily increases, we expect to observe a steady decrease in the value of clearing temperature. This is exactly what is discovered; however, the value of the melting temperature increases proportionally with chain length increasing, which is in good agreement with the experimental result. This is an important finding since the decrease in the clearing temperature must be directly correlated with a significant decline in the order parameter S. Contrariwise, the increase of the melting temperature may be due to the increase of the cohesion molecule caused by the increase of the C–C bond. It is worthwhile to mention that increasing carbon number chain may break the molecular symmetry, so that the formation of the SmF phase is inhibited. Thus, a close inspection of the clearing temperature values for a homologous series may provide an indirect method of evaluating mesophase type in side chain LC.

It should be noted that in complexes with $n = 7$ and 8, the nematic and SmC phases are more stable. The decrease of the SmC range with n increasing can be explained by the fact that when the chain length increases, the strength of the terminal aggregation increases, resulting in the decrease of the smectic range.

3.1.2. Order parameters and birefringence

At the isotropic to nematic transition, the molecules of LCs are statistically oriented along the average direction, which called director, and thereby the molecules have the tendency to rotate about the director, which is called the order parameter (S). We estimate orientational order parameter S from the birefringence data described later and find that all parameters change with chain length increasing. In fact, the order parameter and the birefringence are proportional to the T_{NI} according to the following expressions:[38,39]

$$\Delta n = \Delta n_0 \left(1 - \frac{T}{T_{\mathrm{NI}}}\right)^{\beta}, \tag{1}$$

$$S = \left(1 - \frac{T}{T_{\mathrm{NI}}}\right)^{\beta}, \tag{2}$$

where β is an exponent characteristic of the material, Δn_0 is the birefringence at $T = 0$ K and T_{NI} is the nematic-to-isotropic phase transition temperature (the clearing point). Δn_0 and β are obtained from a fit of Eq. (1) to experimental data (Fig. 5) and regrouped into the four homologues in Table 1.

The experimental data for birefringence of the four compounds are shown in Fig. 5. Increasing the carbon number causes the birefringence to drop slightly from 0.18 to 0.11 at 100 °C.

Table 1. Optical parameters of complexes under study.

Sample	Δn	β
7OBAF	0.23	0.14
8OBAF	0.21	0.11
10OBAF	0.17	0.12
12OBAF	0.16	0.15

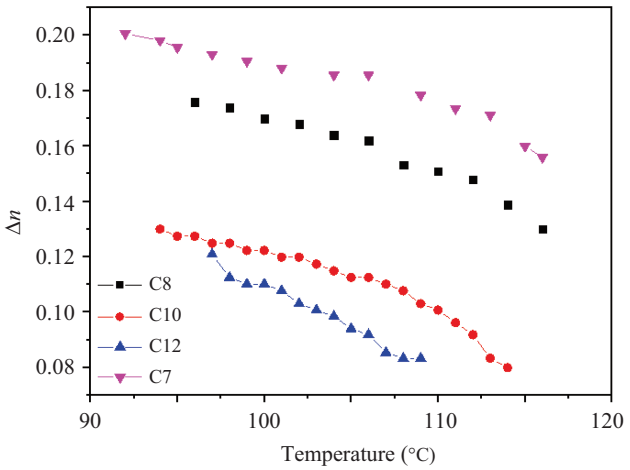

Fig. 5. Temperature-dependent birefringence of complexes under study.

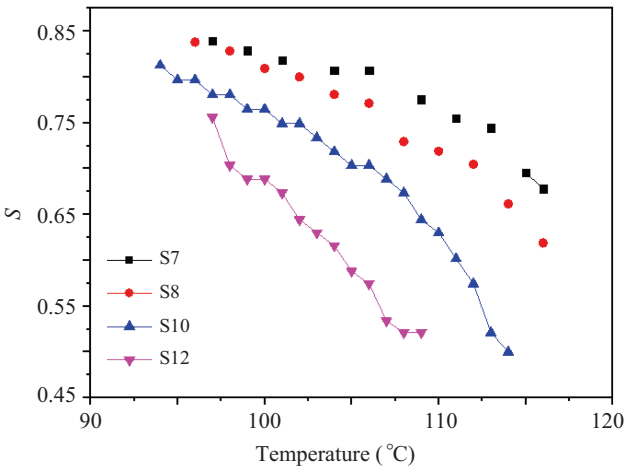

Fig. 6. Temperature-dependent order parameter of complexes under study.

The lower birefringence of the systems is primarily due to the lower clearing points of the systems. High birefringence (Δn) values are expected for the compounds with long chain, as the increasing of chain length may increase the π-electron conjugation through the entire molecule. However, this lowers the birefringence of the compounds, which may be due to the increase of carbon number in flexible chain that traps π-electrons and pull them away from the conjugation along the main molecular axis. Specially, we find that the spontaneous polarization is gradually weakened by increasing the flexible chain length.[17] Here we guess that the bent shape molecule may be deformed by increasing molecule length and the molecule tends to have linear form. Figure 6 shows the curves of order parameter S *versus* temperature for the four compounds. Since T_{NI} decreases with chain length decreasing and S is proportional to this parameter according to Eq. (2), we can confirm that the decrease of T_{NI} with the chain length increasing is due to the decrease of S. Moreover, the order parameter S decreases as temperature increases which is in good agreement with Eq. (2). This reflects the steep temperature variations of various properties exhibited by these compounds, and the fact that the small number of carbon atoms in the chain leads to a relatively high value of the anisotropy of molecular polarizability, which is particularly desirable for elongating the π-electron conjugation through the molecule by increasing the polarizability along the principal molecular axis.

3.2. Nanocomposites $LiNbO_3$/8OBAF

3.2.1. Thermal analysis

Figure 7 presents the DSC thermograms corresponding to pure sample and doped sample. As can be seen, the isotropic–nematic temperature phase transition (T_{N-I}) for the doped sample is lower than for the pure 8OBAF. The T_{N-I} decreases from 116 °C for 8OBAF to 113.2 °C for doped sample. This decrease may be explained by the decrease of the order, which is caused by inserting the NPs in the pure LCs. Owing to the dipole moment, ferroelectric nanoparticles of $LiNbO_3$ generate strong electric fields and interactions around them. Therefore the weak planar anchoring can be induced leading to an easy adaptation of the LCs molecules anchored on the NPs to the surrounding, which in turn reduces the nematic order parameter, and thus reducing the transition temperature. This behavior is consistent with that obtained by our group in the nematic 5CB doped with magnetic NPs.[33] In addition, the decrease of phase transition temperature has been observed in the nematic doped by the gold nanoparticles.[40] Mishra *et al.*[40] have attributed this decrease to the dilution phenomenon. It should be mentioned that the chain length dependence of melting temperature shows a non-universal dependence. Generally, the melting temperature decreases with the increase of the alkyl chain length of liquid crystalline which, in the present case, is consistent with the results in Refs. [28,41], but the melting temperature increases with the number of carbon atoms. Moreover, there appears an odd–even effect of the alkyl chain which has already been observed in several instances.[42,43]

The isotropic–nematic phase transition is also followed by the optical microscopy observations. Figure 8 illustrates the evolution of this transition when the doped sample cooled from the isotropic to nematic phase. At first the small spherical droplets suspended in the isotropic phase and a biphasic

state is observed as shown in Fig. 8(a). After that the droplets grow into different size droplets and the NPs concentrate at the droplet interface. In the case of further cooling, the nematic domain grows to form the point and line defects, where the aggregations are concentrated as shown in Fig. 8(c). This result demonstrates the stable state with the spherical droplets and separate phases without adding any substrate, while some researches have shown that the achievement of this phenomenon implies the presence of surfactant. In addition, the $T_{\mathrm{I-N}}$ decreases from 116 °C for pure compound to 113.2 °C for the doped one. The reduction of $T_{\mathrm{I-N}}$ may be due to the decrease of the order parameter (S) caused by adding the NPs.

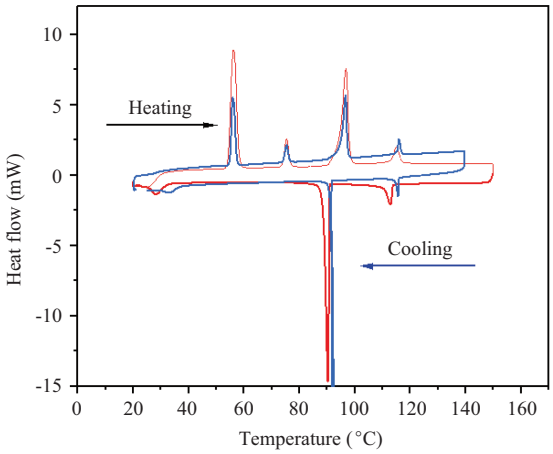

Fig. 7. DSC traces of 8OBAF (blue color) and NPs/8OBABF (red color). Heating and cooling at a rate of 10 °C/min.

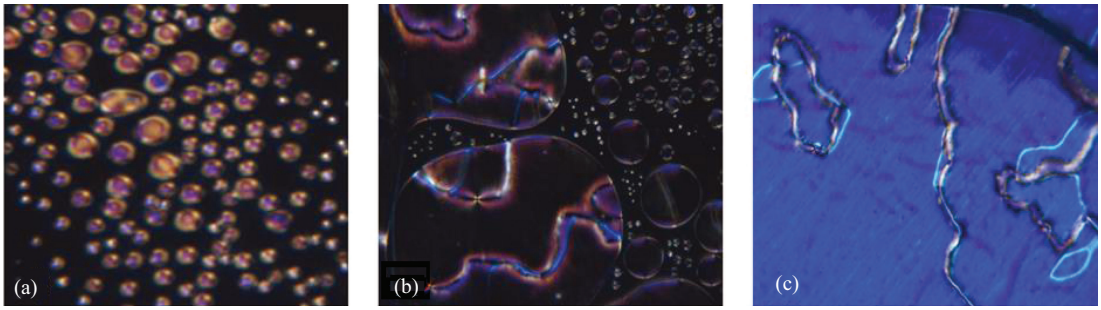

Fig. 8. Optical images of texture of $LiNbO_3$/8OBAF at isotropic–nematic transition.

3.2.2. Dielectric and electrical properties

In order to understand the effect NPs on the electrical and dielectric behaviors, the real part (ε') and imaginary part (ε'') of dielectric permittivity are measured by using the impedance/gain phase analyzer (Solartron SI1260) in a frequency range from 20 Hz to 10 MHz.

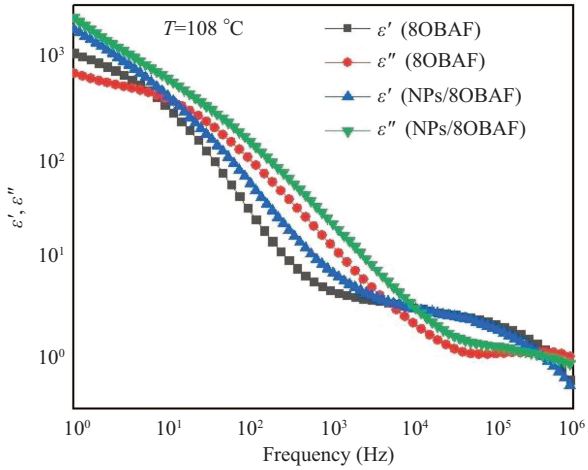

Fig. 9. Frequency-dependent $\varepsilon'(f)$ and $\varepsilon''(f)$ for 8OBAF and NPs/8OBAF.

Figure 9 shows these frequency-dependent parameters in nematic phase at 108 °C. The increase of dielectric permittivity (ε' and ε'') due to the dispersion of the NPs is clearly observed. This result indicates that the presence of the $LiNbO_3$ enhances the conductivity of the nanocomposites. It should be mentioned that this behavior have already been observed in Ref. [36].

In addition, both the real (Z') element and imaginary (Z'') element of the complex electrical impedance (Z^*) are measured in a frequency range of 1 Hz–10 MHz. Therefore, an equivalent electric circuit (EEC) model is proposed in order to analyze the impedance spectrum (Fig. 10). The EEC model can be simplified as follows: the resistor for the resistivity of the cell's electrodes and connectors (R_{CR}, in series with a parallel set of C_{LC} capacitors and R_{LC} resistor, approximating the active and reactive behavior of the LCs, Sprokel[44] have added capacitance element C_{DL} in series to C_{LC} and R_{LC} to model low frequency behavior in a region of 1 Hz–100 Hz, and Zafra *et al.*[45] have included a finite diffusion Warburg element, W, connected in parallel to C_{DL} to represent the drift of charged species near the electrode. The impedance of the Warburg element can be written as[46]

$$Z_W = \frac{W_{\mathrm{sr}}}{\sqrt{\omega}}(1-\mathrm{j})\tanh(W_{\mathrm{sc}}\sqrt{\mathrm{j}\omega}). \tag{3}$$

The coefficients W_{sr} and W_{sc} can be expressed as

$$W_{\mathrm{sr}} = \frac{RTN_{\mathrm{A}}}{F^2An_{\mathrm{s}}\sqrt{2D}}, \tag{4}$$

$$W_{\mathrm{sc}} = \frac{\delta_{\mathrm{N}}}{\sqrt{D}}, \tag{5}$$

where T is the temperature expressed in Kelvin, R is the gas constant, N_A is the Avogadro's number, F is the Faraday constant, A is the surface area, n_s is the surface concentration of the ions, and δ_N is the thickness of the Nernst diffusion layer. The fitting parameters are listed in Table 2.

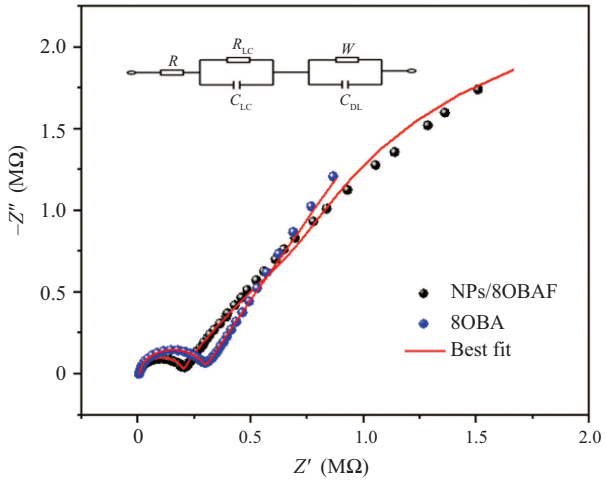

Fig. 10. Nyquist plots of 8OBAF and $LiNbO_3$/8OBAF nanocomposites.

As seen in Table 1, the presence of $LiNbO_3$ NPs in 8OBAF increases the capacitive effects of the C_{DL} and reduces the bulk resistance R_{LC}. The value of the double layer capacitance C_{DL} is very higher than that of the bulk capacitance C_{LC}, which is in good agreement with that obtained for 5CB doped by gold nanoparticles.[47] On the other hand, the increment in C_{DL} by $LiNbO_3$ NPs in our case can be attributed to the enhancement of the space charge motion, therefore the ion moves easily toward the electrode. This is consistent with the decrement in W_{sr} due to the increase of the diffusion coefficient according to Eq. (4). It should be mentioned that this behavior is quite useful because the presence of $LiNbO_3$ NPs increases the conductivity and reduces the resistivity of the system. Indded, the bulk resistance decreases from 2.83 MΩ for the 8OBAF to 1.92 MΩ for the doped sample as shown in Table 2, while, the conductivity increases from 0.75×10^{-6} m·s^{-1} for the pure sample to 1.3×10^{-6} m·s^{-1} for the doped one at 1 kHz and 105 °C. This behavior can be explained by the decrease in the rotaional viscosity and response time when 8ONAF is doped by $LiNbO_3$ NPs. We have reported in our previous work on the influence of $LiNbO_3$ on the electro–optic behavior of the 8OBAF and found that the rotational viscosity decreases from 50 mPa·s for undoped 8OBAF to 7 mPa·s for 8OBAF + 1% NPs and the response time decreases from 16 ms for undoped 8OBAF to 8 ms for 8OBAF + 1% NPs.[35] As consequence the space charge motion is enhanced leading to the bulk resistance to decrease and the conductivity to increase.

Table 2. Impedance spectroscopy parameters of elementsin EEC model obtained from measured impedance spectra.

Samples	R_{CR} (kΩ)	R_{LC} (MΩ)	C_{LC} (pF)	C_{DL} (pF)	W_{sr} (MΩ·s$^{-1/2}$)	W_{sc} (Ω·s$^{-1/2}$)
8OBAF	5.9	2.83	1.75	5.01	8.03	0.60
NPs/8OBAF	4.7	1.92	1.09	9.4	4.61	0.480

4. Conclusions

A new series of fluorinated hydrogen bonded liquid crystals from 4-*n*-alkoxybenzoic acid (*n*OBAF) is studied by using the POM, DSC, and dielectric technique. The DSC and POM show that the enantiotropic SmF, which is depressed in the compound with a long chain length. It is found that the clearing temperature decreases with chain length increasing. Moreover, all the compound contains the nematic and SmC phase. On the other hand the influence of $LiNbO_3$ on the isotropic–nematic phase transition for the 8OBAF is investigated. This transition reveals the formation of the spherical droplets and the decrease of the temperature transition. In addition the presence of the nanoparticles increases the conductivity and reduces the resistivity of the doped sample.

References

[1] Alaasar M, Poppe S and Tschierske C 2019 *J. Mol. Liq.* **277** 233
[2] Cho C M, Wang X, Li J J, He C and Xu J 2013 *Liq. Cryst.* **40** 185
[3] Martinez-Felipe A, Cook A G, Abberley J P, Walker R, Storey J M and Imrie C T 2016 *RSC Adv.* **6** 108164
[4] Alaasar M, Schmidt J C, Darweesh A F and Tschierske C 2020 *J. Mol. Liq.* **310** 113252
[5] Alaasar M, Tschierske C and Prehm M 2011 *Liq. Cryst.* **38** 925
[6] Al Sheikh Ali A, Khan D, Naqvi A, Al-Blewi F F, Rezki N, Aouad M R and Hagar M 2020 *ACS Omega* **6** 301
[7] Almehmadi M A, Aljuhani A, Alraqa S Y, Ali I, Rezki N, Aouad M R and Hagar M 2021 *J. Mol. Struct.* **1225** 129148
[8] Armstrong G and Buggy M 2005 *J. Mater. Sci.* **40** 547
[9] Blanke M, Balszuweit J, Saccone M, Wölper C, Jiménez D D, Mezger M, Voskuhl J and Giese M 2020 *Chem. Commun.* **56** 1105
[10] Bryndal I, Drozd M, Lis T, Zaręba J K and Ratajczak H 2020 *CrystEngComm* **22** 4552
[11] Chen S, Jiang S, Qiu J, Guo H and Yang F 2020 *Chem. Commun.* **56** 7745
[12] Gimeno N, Ros M B, Serrano J L and De La Fuente M R 2004 *Angew. Chem.* **116** 5347
[13] Mohan M M 2021 *IOP Conf. Ser.* 012089
[14] Fouzai M, Guesmi A, Hamadi N B and Soltani T 2020 *Liq. Cryst.* **47** 777
[15] Hagar M, Ahmed H, El-Sayed T and Alnoman R 2019 *J. Mol. Liq.* **285** 96
[16] Devadiga D and Ahipa T 2020 *Liq. Cryst. Rev.* **8** 5
[17] Nguyen H L, Horton P N, Hursthouse M B, Legon A C and Bruce D W 2004 *J. Am. Chem. Soc.* **126** 16
[18] Missaoui T, Amor I B, Soltani T, Ouada H B, Jeanneau E and Chevalier Y 2020 *J. Mol. Liq.* **304** 112726
[19] Paleos C M and Tsiourvas D 2001 *Liq. Cryst.* **28** 1127

[20] Parveen S, Hagar M B, Alnoman R, Ahmed H A, El Ashry E S H and Zakaria M A 2021 *Polycyclic Aromatic Compounds* 1

[21] Arakawa Y, Sasaki Y and Tsuji H 2019 *J. Mol. Liq.* **280** 153

[22] Walker R, Pociecha D, Crawford C A, Storey J M, Gorecka E and Imrie C T 2020 *J. Mol. Liq.* **303** 112630

[23] Walker R, Pociecha D, Abberley J, Martinez-Felipe A, Paterson D, Forsyth E, Lawrence G, Henderson P, Storey J and Gorecka E 2018 *Chem. Commun.* **54** 3383

[24] Moirangthem M and Schenning A P 2018 *Polycyclic Aromat. Compd.* **10** 4168

[25] Li Y, Zhuo H, Chen H and Chen S 2019 *Polymer* **179** 121671

[26] Ni B, Xie H L, Tang J, Zhang H L and Chen E Q 2016 *Chem. Commun.* **52** 10257

[27] Ban J, Mu L, Yang J, Chen S and Zhuo H 2017 *J. Mater. Chem. A* **5** 14514

[28] Hagar M, Ahmed H A, Alnoman R B, Jaremko M, Emwas A H, Sioud S and Al-Ola K A 2021 *Front. Chem.* 9

[29] Yan X, Zhou Y, Liu W, Liu S, Hu X, Zhao W, Zhou G and Yuan D 2020 *Liq. Cryst.* **47** 1131

[30] Pushpavathi N, Sandhya K and Pratibha R 2019 *Liq. Cryst.* **46** 666

[31] Ayeb H, Alaya S, Derbali M, Samet L, Bennaceur J, Jomni F and Soltani T 2021 *Liq. Cryst.* **48** 223

[32] Chemingui M, Singh U B, Yadav N, Dabrowski R S and Dhar R 2020 *J. Mol. Liq.* **319** 114299

[33] Ayeb H, Derbali M, Mouhli A, Soltani T, Jomni F, Fresnais J and Lacaze E 2020 *Phys. Rev. E* **102** 052703

[34] Nasri R, Missaoui T, Hbibi A and Soltani T 2021 *Liq. Cryst.* 1

[35] Derbali M, Guesmi A, Hamadi N B and Soltani T 2020 *J. Mol. Liq.* **319** 113768

[36] Lalik S, Deptuch A, Jaworska-Gołłą B T, Fryń P, Dardas D, Stefanczyk O, Urbańńska M and Marzec M 2020 *J. Phys. Chem. B* **124** 6055

[37] Fouzai M, Hamdi R, Ghrab S, Soltani T, Ionescu A and Othman T 2018 *J. Mol. Liq.* **249** 1279

[38] Selvaraj P, Subramani K, Hsu C J and Huang C Y 2020 *Polymers* **12** 2977

[39] Basumatary J, Nath A and Devi T K 2020 *J. Mol. Liq.* **311** 113251

[40] Mishra R, Hazarika J, Hazarika A, Gogoi B, Dubey R, Bhattacharjee D, Singh K N and Alapati P R 2018 *Liq. Cryst.* **45** 1661

[41] Wang X, Sternberg M, Kohler F T, Melcher B U, Wasserscheid P and Meyer K 2014 *RSC Adv.* **4** 12476

[42] Luo C C, Jia Y G, Song K M, Meng F B and Hu J S 2017 *Liq. Cryst.* **44** 2366

[43] Yamamura Y, Tsuchiya R, Fujimura S, Hishida M and Saito K 2017 *J. Phys. Chem. B* **121** 1438

[44] Sprokel G 1974 *Mol. Cryst. Liq. Cryst.* **26** 45

[45] Zafra J C T, Garcilópez I A P, Del Pozo V U, Pena J M S and Lucas C M 2011 *Opt. Eng.* **50** 081206

[46] Seo J H, Huh J W, Sohn H J, Lim E and Yoon T H 2020 *Cryst.* **10** 55

[47] Urbanski M and Lagerwall J P 2017 *J. Mater. Chem. C* **5** 8802